RESEARCH

Compact dual-port MIMO filtenna-based DMS with high isolation for C-band and X-band applications

Rania H. Elabd[1]*

*Correspondence:
Eng.rania87@yahoo.com;
rania.hamdy@ndeti.edu.eg

[1] Electronics
and Communications
Engineering Department,
High Institute of Engineering
and Technology, New Damietta,
Egypt

Abstract

A dual-port multiple-input multiple-output (MIMO) filtenna with minimal sizes of 80×45 mm^2 is set up in this study. Each element in this MIMO filtenna is positioned orthogonally to the one next to it to improve isolation. For the MIMO element to achieve high-frequency selectivity and compact size, a frequency-reconfigurable filtenna that was created by fusing a band-pass filter and a monopole radiator was used. The suggested filtenna can switch between its C-band and X-band operating states with ease. On build the filtenna circuit, a band-pass filter based on defective microstrip structure is inserted to a circular monopole radiator. The developed filtenna operates in the C-band frequency range of 6.5–8 GHz and the X-band frequency range of 8–12 GHz. It is possible to use the X-band operating state for communication in a cognitive radio environment. Used as a decoupling structure, metamaterial structures can increase isolation to more than 40 dB across the bandwidth. The suggested MIMO filtenna system has an envelope correlation coefficient of 2.4e−6, a peak gain of 6 dBi, and an impedance bandwidth of 7.4–7.75 GHz. The MIMO filtenna is constructed and measured, and the findings of the measurement and simulation are in good agreement.

Keywords: C-band, DMS, DS, ECC, Filtenna, Metamaterial, MIMO, X-band

1 Introduction

In order to replace the need of several antennas resonating at different frequencies, the small antenna must be equipped with on-demand frequency reconfigurability due to the rapid advancement of the various technologies [1]. The frequency ranges employed by common technologies including WLAN (5.15–5.85 GHz), WiMax (3.3–3.7 GHz), C-band (4–8 GHz), and X-band communication satellites (7.25–7.75 GHz) for space-to-earth communication and (7.9–8.4 GHz) for space-to-space communication [2]. Front ends for conventional RF communication systems include a receiver antenna, a mixing circuit, and a band-pass or bandstop filter. The enormous size of the circuit components, the bulky design, and the mismatch between the circuits components are some of the issues with these systems. Overcoming the disadvantage of employing distinct circuits is crucial for the progress of contemporary

ultra-wideband communication schemes that are meant to be employed in contemporary communication networks. The so-called filtenna structure integrates the antenna with the necessary filters as a beautiful solution to this design dilemma [3].

High-speed ADCs are necessary for wideband antennas, but they use a lot of power and have larger quantization errors. Finally, because of constraints in the RF front-end components like amplifiers, oscillators, and mixers, the design for wideband operation compromises the transceiver performance. Narrowband frequency adjustable antennas, also known as tunable filter-antennas, are suitable candidates for use in order to sense the frequency spectrum due to all the aforementioned problems. This is due to the flexible frequency discrimination, wideband suppression of unwanted interference, gain flatness over the operating frequency band, less interference with the antenna's radiation characteristics, improved processing of down-converted signals, simplicity of implementation, and high performance of tunable band-pass filtering [4]. Due to their straightforward construction, patch and monopole antennas have been used by researchers for conformal applications. However, their disadvantageous size prevents them from being used for tiny devices [5, 6]. By incorporating dissimilar open-ended or short-ended stubs and slots into radiating constructions, the antenna size has been decreased. However, it adds structural complexity, which causes problems during fabrication [7]. In order to increase capacity, achieve diversity, improve the multipath effect, or minimize channel fading, MIMO techniques have been implemented in communication schemes [8–11]. Another way to increase capacity discrete wavelet transforms (DWT), DWTs are employed in orthogonal frequency division multiplexing (OFDM) systems to improve spectral efficiency. Therefore, wavelet transforms can be used to design antenna diversity scheme to improve performance of system and spectrum efficiency [12–18].

MIMO antenna design and deployment must take into account two key needs. These include constructing the antenna with the highest possible isolation between antenna elements and sizing it appropriately for portable applications. A good reception strategy is made possible by the strong isolation, which results in low mutual coupling (MC) between antennas [19]. It is well known that as the array size grows, the degree of coupling also grows. To lessen the MC in the MIMO antennas, many topologies and structures have been devised. The literature has discussed polarized orthogonal elements [20, 21], electromagnetic band-gap (EBG) structure [22], meander-line EBG [23], neutralization line [24, 25], stubs [26, 27], parasitic elements [28, 29], shorting pin [30], metamaterials with neutralization lines [31, 32], slots, or carbon black film [33]. Chen et al. [20] It describes a MIMO system with two orthogonal polarized antenna elements that has dimensions of 27×21 mm^2 and a 22.5 dB isolation level. Authors of [22] introduced a quad-port double-side MIMO antenna. It is reliant on EBG structure and was created to enhance isolation. The MIMO system consists of four polygonal parts. Additionally, a 30×30 mm^2 FR4 substrate with a partly slotted EBG stub-ground is also comprised. A meander-line EBG construction has been employed in [23] to reduce MC between two 32×64 mm^2 antenna elements. So as to absorb the antenna interference, a carbon black layer was used in [33] to increase the amount of isolation. Achieved were $S_{21} < -15$dB and envelope correlation coefficients < 0.02. All prior designs, however, had problems with either excessive bulk or inadequate isolation.

The described works either have the drawbacks of solid substrates, greater dimensions, or set working frequencies, to wrap up this debate. As a result, this work makes two contributions. The first is the design and construction of a filtenna element with a circular base. This design is suggested because it creates a tiny antenna, conformal, and has on-demand frequency-switching between the thirteen different bands, which are used for C-band and X-band applications. It also gives a longer electrical line in a small space. For the purpose of preventing potential electromagnetic interference with other systems, the antenna provides harmonic suppression up to 12 GHz. The introduction of a dual-port MIMO filtenna with exceptional port-to-port separation follows. The MIMO construction is built using an orthogonal filtenna design to lessen element-to-element coupling. Inserting a metamaterial with a zigzag shape between adjacent parts further improves isolation. The MC effectively increases port-to-port isolation to more than 40 dB among the two ports across the majority of the working bandwidth when this zigzag shape is positioned between the antenna elements. This results in an overall size of 80×45 mm^2. The structure of this essay is as follows. Method and experiment is described in Sect. 2. The tunable filtenna design process is described in Sect. 3. The MIMO filtenna system is discussed in Sect. 4 along with a demonstration of how to use a metamaterial to lower the isolation level. Section 5 presents the results and discussion. The paper is concluded in Sect. 6.

2 Method and experiment

Figure 1 shows the processes of the methodology for designing a dual-port MIMO filtenna. The MIMO filtenna and antenna element is simulated using the CST program. Each element in this MIMO filtenna is positioned orthogonally to the one next to it to improve isolation. To provide further isolation between the antennas ports, a DS between the antennas is added into the top layer.

3 Tunable filtenna design procedure

3.1 Wideband antenna design

A design for a WB circular patch antenna element based on partial ground structure is introduced in this subsection and is depicted in Fig. 2. A Rogers RT5880 substrate with a dielectric constant ε_r of 2.2, a tan δ of 0.0009, and a thickness h of 1.52 mm is used to print the antenna structure. The design was created using the software program microwave studio for computer simulation technology (CST). Table 1 contains the antenna's dimensions in millimeters. A feeding line with a width of W_f connects the patch to a 50 Ω SMA connection. Figure 3a shows the simulation of the reflection coefficient $|S_{11}|$ versus frequency. It is obvious that the suggested antenna covers a broad frequency range from 2.4 to more than 12 GHz for $|S_{11}| \leq -10$ dB.

According to Fig. 3b, the simulated antenna efficiency spans the full operating frequency band and is between 80 and 99%. In addition, as presented in Fig. 3c, the antenna's simulated realized gain spans the working frequency band from 2.2 to 5.9 dB.

Figure 4 depicts the manufactured prototype of the suggested wideband antenna. As illustrated in Fig. 5, the suggested wideband antenna's scattering parameter $|S_{11}|$ is measured using a Rohde & Schwarz ZVB 20 vector network analyzer. In the entire frequency range from 2.4 GHz to more than 12 GHz, the $|S_{11}|$ is below the -10 dB. The simulated
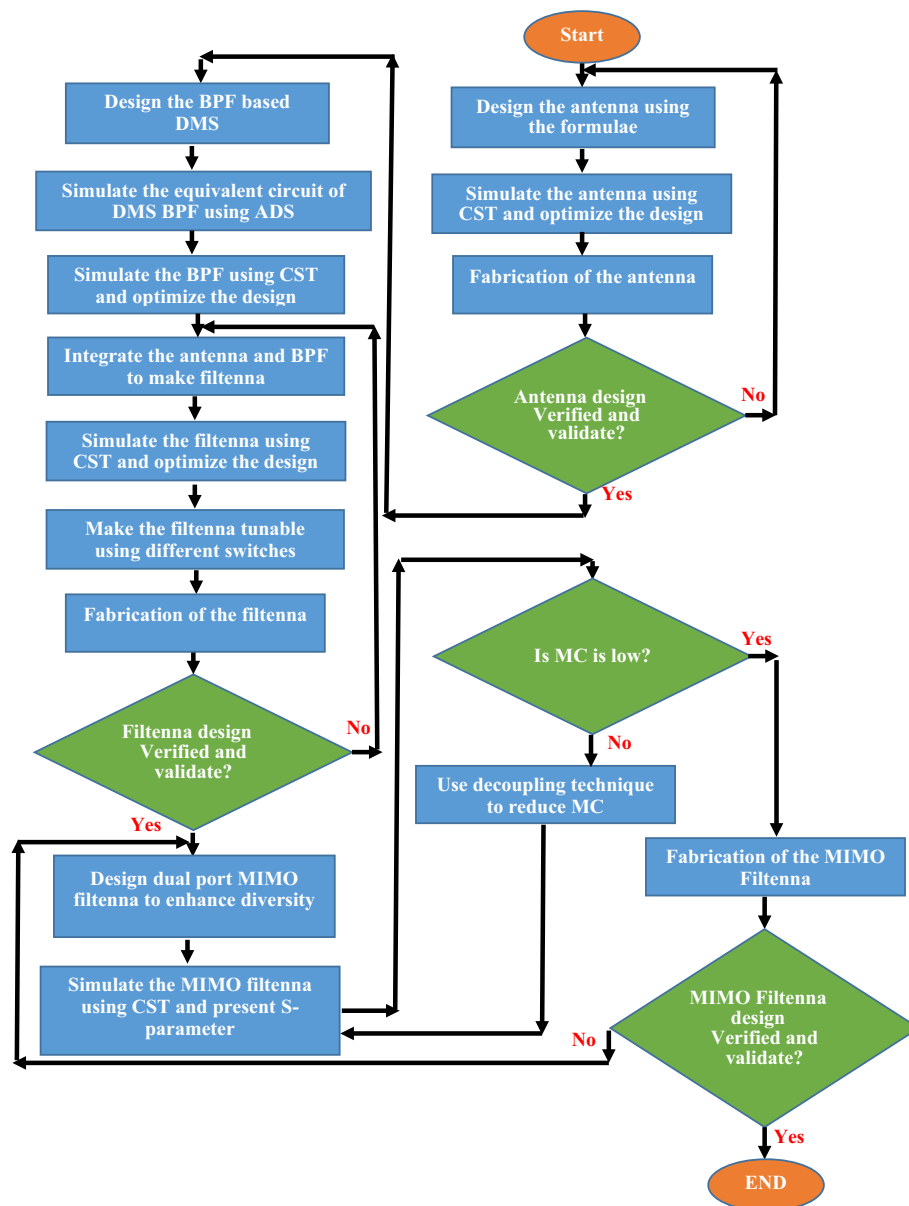
Fig. 1 Methodology steps to design the dual port MIMO filtenna

and measured findings show a good degree of consistency. However, there is not much of a difference between the modeling and measurement results because of manufacturing tolerance levels.

3.2 Design of the proposed BPF-based DMS

In this subsection, the design of the planned BPF is presented. It is based on using of defected microstrip structure (DMS) technique. Firstly, a two tinny slit is etched at the midpoint of the stripe line, separating them from each other by 0.5mm which act as a fixed capacitance as displayed in Fig. 6. Secondly, a U-shaped slot of dimension 4.69 mm × 0.86 mm is etched at the middle part of strip line to control the coupling between

Fig. 2 Proposed WB antenna element structure **a** front view and **b** back view

Table 1 Dimensions of the proposed WB antenna element in mm

Dimension	mm	Dimension	mm
W	45	L_f	16
L	35	L_g	14.7
W_f	5.47	L_c	3.7
R	13	W_c	5.47
R_c	2		

the two transmission line sections. The purpose of the gaps is to allow the filter to have the "band-pass" feature by functioning as a parallel-series resonance.

The DMS construction can be expressed in terms of lumped elements by using circuit theory. The design is simulated with computer simulation technology (CST) software. So as to extract each of the different resonant frequencies, the S-parameters matrix obtained is then exported to the advanced design system (ADS). According to [34], the corresponding values for the capacitances and the inductances can be obtained from the next two equations.

$$C_{s,p} = \frac{f_c}{200\pi \left(f_o^2 - f_c^2\right)}, \ L_{s,p} = \frac{1}{4\pi^2 f_o^2 C_{s,p}}$$

where f_o is the resonant frequency and f_c is the cutoff frequency of the designed filter. The change in the values of C and, the filter operating frequency will change.

Figure 7 displays the equivalent circuit model for the DMS filter. The two gaps are modeled as parallel series LC and are represented by the inductor L_s and the capacitor C_s, and the U-slot is modeled by L_p and C_p. Figure 8a shows the simulated scattering parameter for DMS equivalent circuit in ADS simulation program. It is noticed that the behavior of the BPF is ideal and allows to pass frequency 7.6 GHz at specified value of of
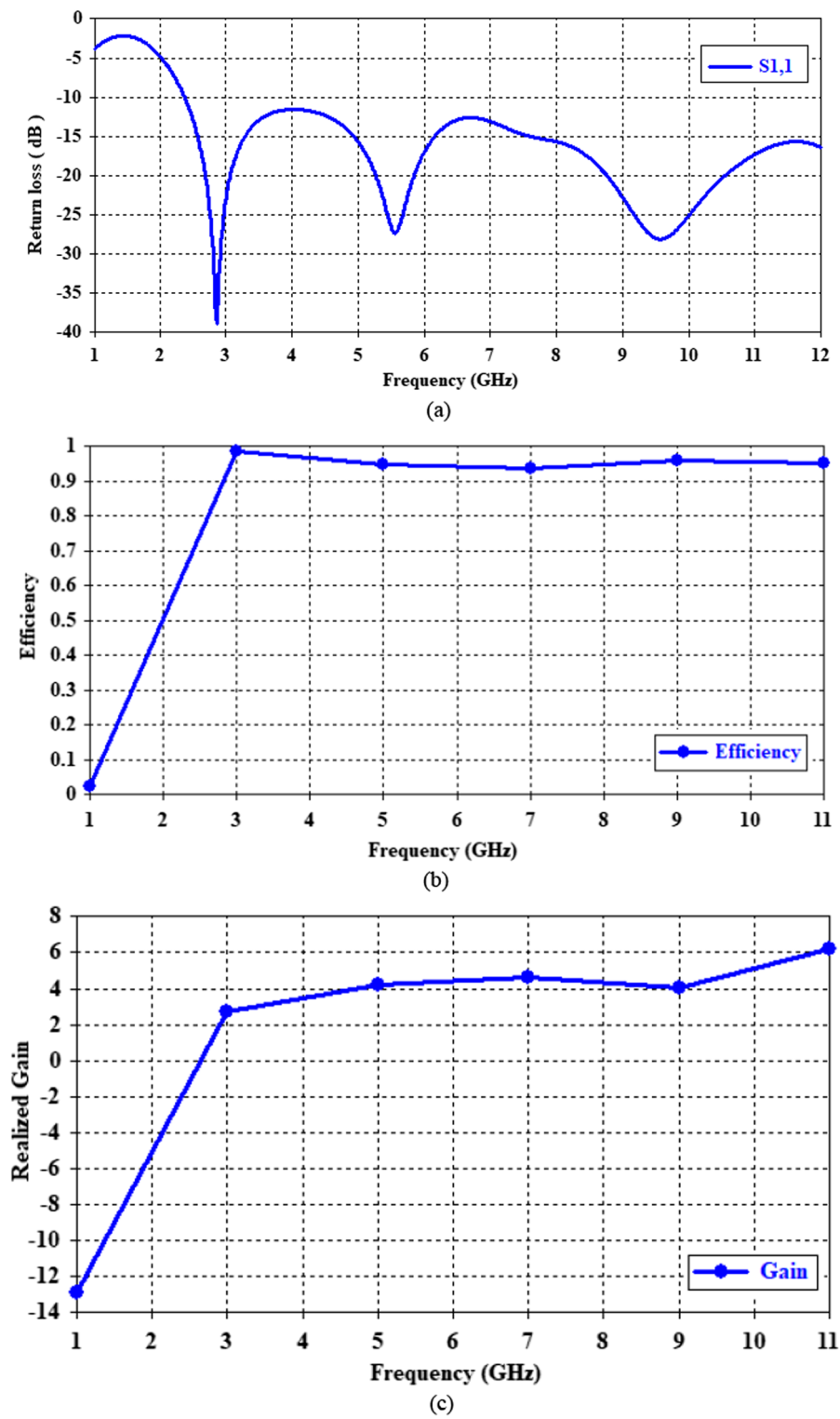
Fig. 3 Simulated parameter of the WB antenna element. **a** $|S_{11}|$, **b** efficiency, and **c** gain
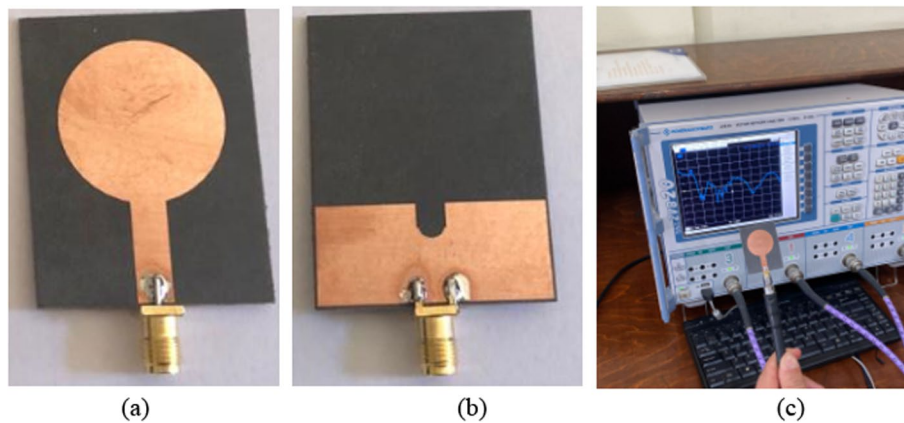
Fig. 4 Fabrication of the proposed wideband antenna **a** top view, **b** bottom view, and **c** S-Parameters measurement setup
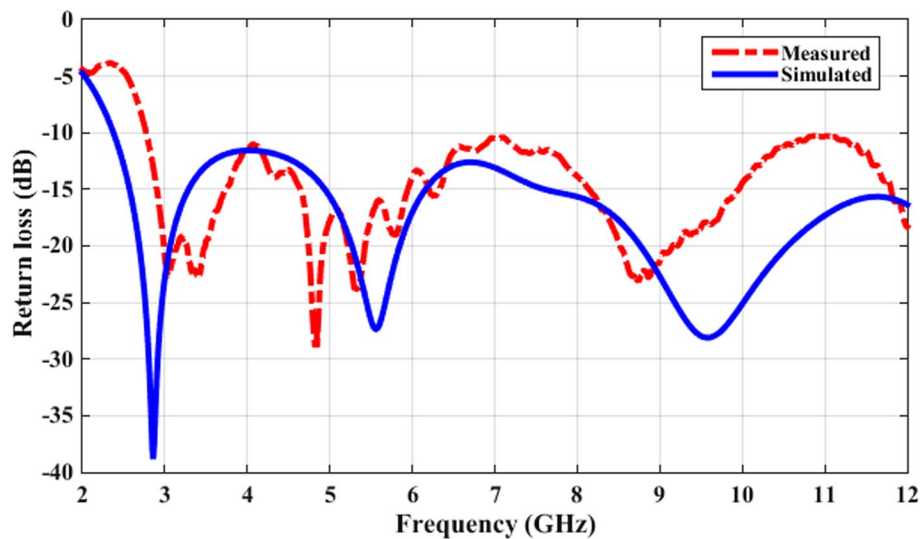

Fig. 5 The simulated and measured reflection coefficient $|S_{11}|$ of the proposed wide band antenna element

C and L as presented in Fig. 7. Figure 8b presents the simulated Scattering parameter for the proposed DMS BPF. It is noticed that S_{11} is below -10dB at frequency 7.6 GHz and insertion loss is -1.8dB.

3.3 Frequency-reconfigurable filtering antenna

In this subsection, the design of the suggested tunable filtenna is presented. As shown in Fig. 9a, the BPF based on DMS is etched in the feed line of the WB antenna to create the filtenna. Impedance matching among the radiating patch and the BPF is made easier by this configuration while reducing system size and expense. To achieve reconfigurabitly and get variable frequencies, there are eight switches at different places in filtenna construction as shown in Fig. 9b. A comparison between the simulated $|S_{11}|$ versus frequency of the antenna and the suggested filtenna is plotted in Fig. 10a. It is noted that the combination of the BPF with the antenna enables the wide band
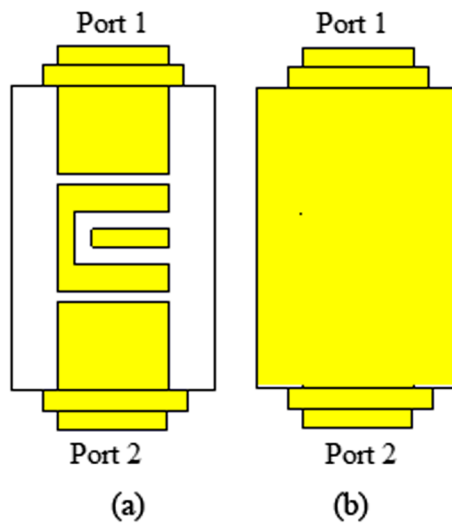
Fig. 6 Proposed DMS-BPF structure **a** front view and **b** back view
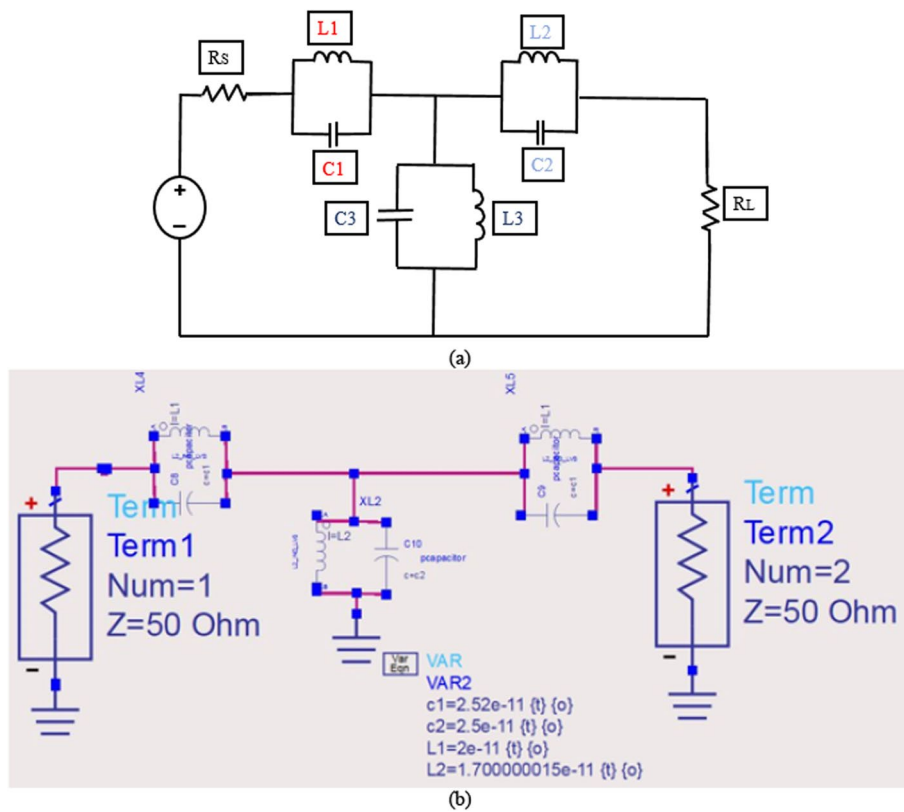

Fig. 7 **a** The equivalent circuit model for the DMS reconfigurable filter. **b** The Schematic circuit model in ADS simulation program

antenna to operate at a narrowband state with high selectivity. While the simulated $|S_{11}|$ versus frequency of the tunable filtenna at various tuning switches is shown in Fig. 11. The achieved tuning frequency band is 5.55GHz, which spans the range from
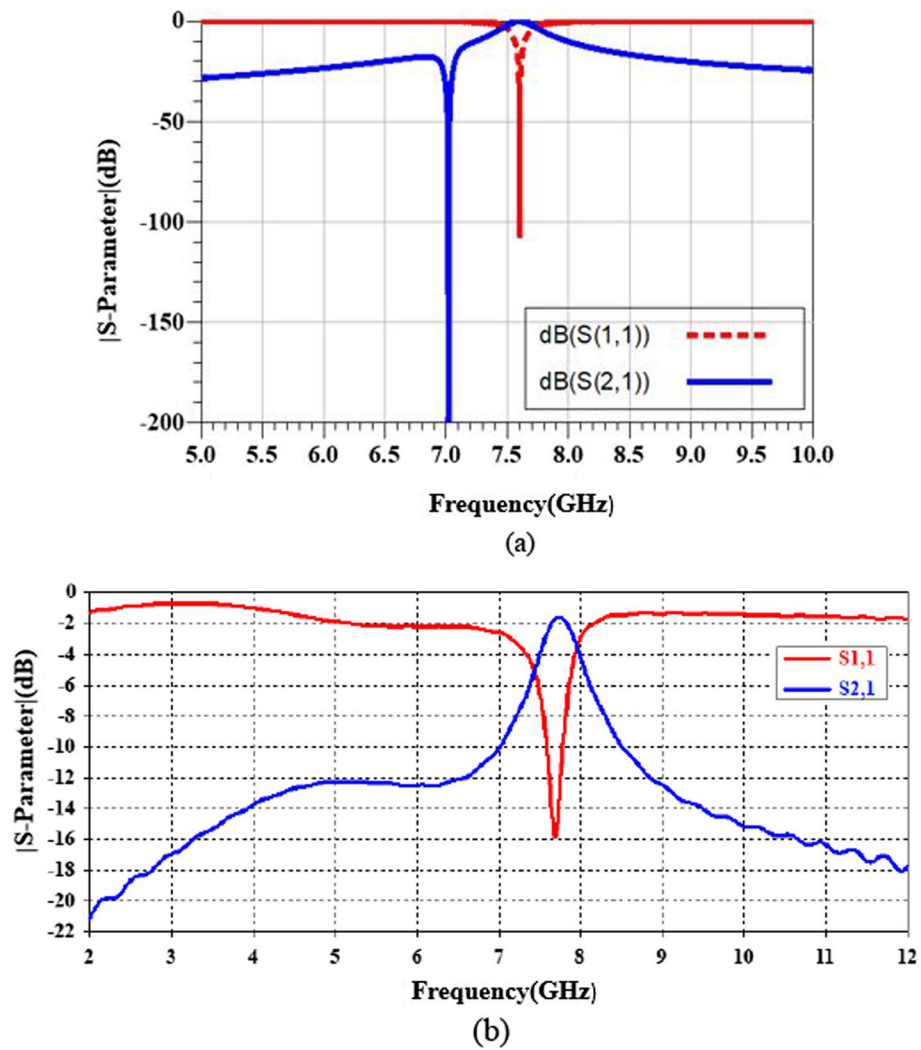
Fig.8 Simulated scattering parameter of **a** DMS equivalent circuit in ADS simulation program. **b** Proposed BPF-based DMS
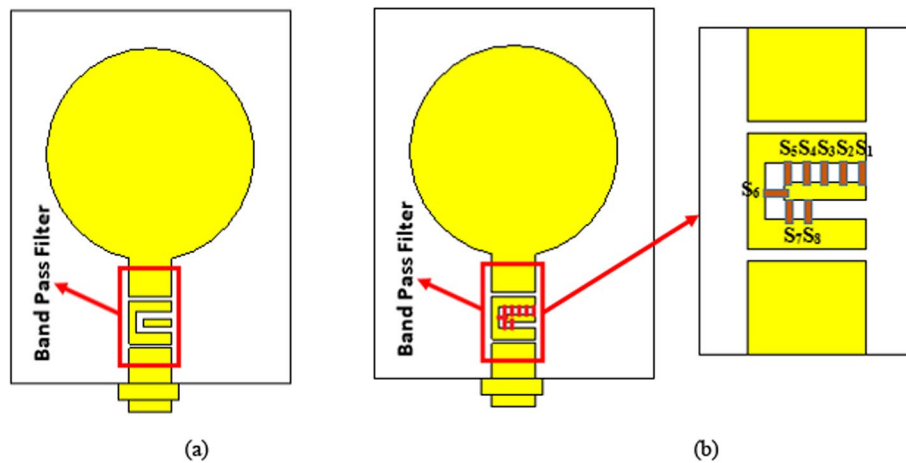

Fig. 9 a Front view of Suggested filtenna construction. **b** Front view of Suggested tunable filtenna construction with different switches
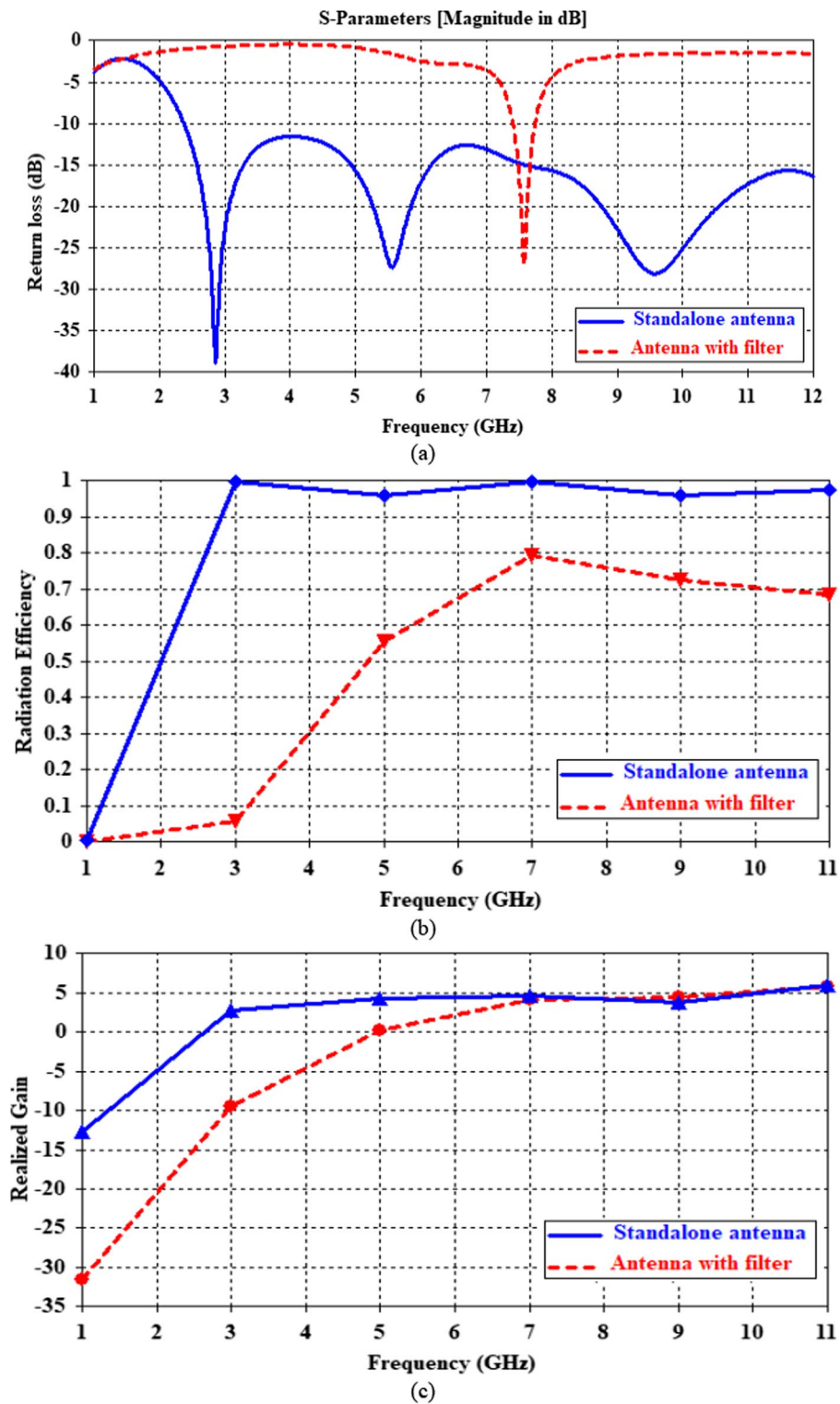
Fig. 10 Simulated parameter of the standalone antenna and antenna with filter. **a** $|S_{11}|$, **b** efficiency, and **c** gain
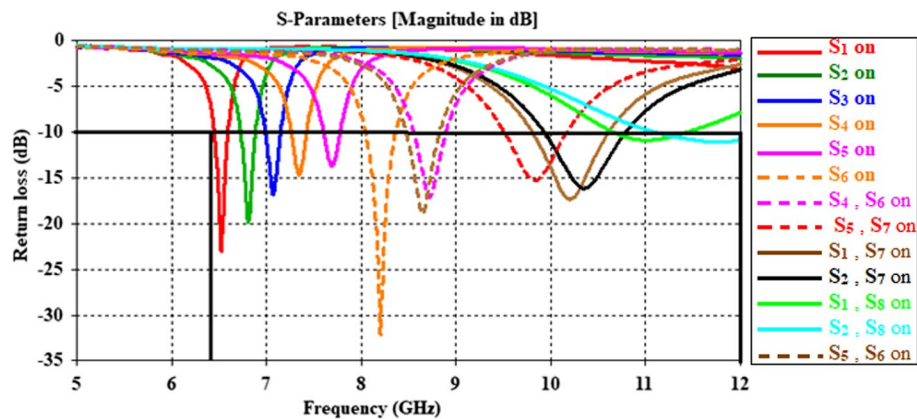
Fig. 11 Simulated return losses $|S_{11}|$ of the suggested filtenna at different states of the switches

Table 2 The effectiveness of the suggested filtenna at different states of the switches

Case of switches	Modes $S_8S_7S_6S_5S_4S_3S_2S_1$	Resonating frequency (GHz)	Operational bandwidth (GHz)	10dB BW (MHz)	Efficiency (%)	Realized gain (dBi)
All off	00000000	7.578	7.4–7.75	37.7	77.5	4.2
S_1 on	00000001	6.526	6.45–6.59	17.3	79.9	3.02
S_2 on	00000010	6.813	6.73–6.89	18.4	80.6	3.8
S_3 on	00000100	7.072	6.99–7.15	18.4	81.1	3.9
S_4 on	00001000	7.345	7.26–7.43	19.5	71.5	3.7
S_5 on	00010000	7.695	7.6–7.77	19.5	74	4.46
S_6 on	00100000	8.213	8.04–8.38	33.9	68	3.9
S4, S6 on	00101000	8.654	8.47–8.83	36	71.8	3.77
S5, S7 on	01010000	8.732	8.55–8.89	35.6	76.2	3.9
S1, S7 on	01000001	9.837	9.51–10.2	68.3	80.2	4.1
S2, S7 on	01000010	10.215	9.8–10.6	80.4	82.4	4.3
S1, S8 on	10000001	10.335	9.92–1079	88.2	72.9	5.7
S2, S8 on	10000010	11.02	10.22–11.9	84.9	72.5	6.3
S5, S6 on	00110000	11.776	10.44–12.6	94	70.5	5.8

1 tends to switch on, 0 tends to switch off

6.45GHz to more than12GHz. The result of the changing state of switches, operational bandwidth (GHz), 10dB BW, efficiency, and realized gain (dBi) of the suggested filtenna is depicted in Table 2. It is evident that the filter has high selectivity with narrow bandwidths ranging from 17.3to94MHz over the entire tuning modes. Figure 10b, c provides clarification on the impact of the BPF's insertion loss, and switches, on the filtenna's efficiency and realized gain in*dBi*. The realized gain and efficiency of the filtenna ranged from 3 to 5.8dBi and 68–82.4%, respectively, within the tuning range.

A sample prototype of the planned filtenna at different states of the switches was fabricated using a standard chemical etching process to validate the design concept. Figure 12 shows the top side of the fabricated prototype at different states of the switches.

The comparison among simulated and measured reflection coefficients of the proposed antenna for various switching cases is plotted in Fig. 13.
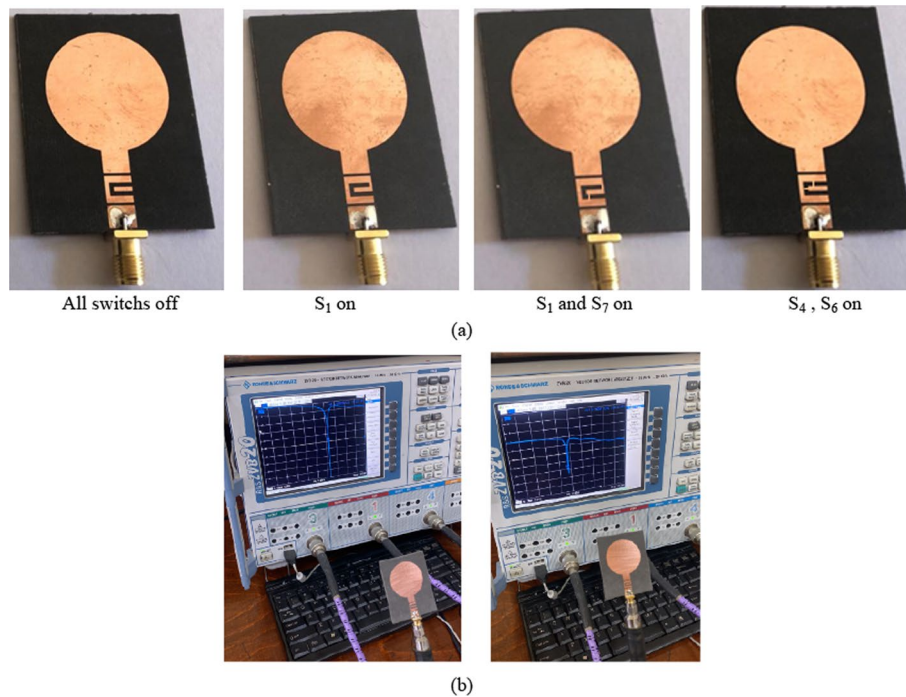
All switchs off S_1 on S_1 and S_7 on S_4 , S_6 on

(a)

(b)

Fig. 12 a Fabricated prototype of the proposed filtenna at different states of the switches. **b** The setup for measuring S-Parameters
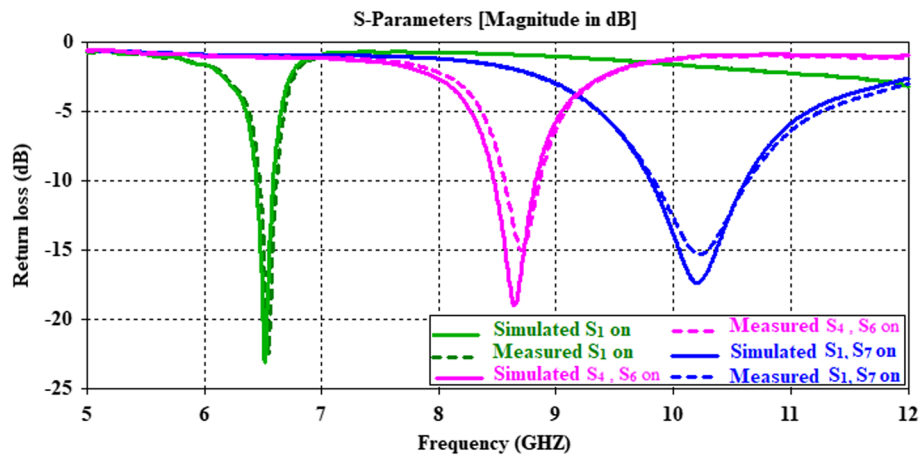

Fig.13 A comparison between the simulated and measured $|S_{11}|$ of filtenna at different states of the switches

When switch S_1 was kept on, while the other switches were kept in off-state (Case-00000001), the antenna resonated at 6.55 GHz, with a measured fractional bandwidth of 2.13%, ranging from 6.47 to 6.61GHz. On the other hand, when switches S_4 and S_6 were kept on, while the other switches were kept in off-state (Case-00101000), the antenna gave a resonance at 8.654 GHz, having measured $|S11| < -10$ dB impedance bandwidth of 4.15% (8.47–8.83GHz).Similarly, keeping switch S_1 in on-state, when S_7 was kept on, and while keeping the others in off-state, then the antenna operated at 9.837GHz

Table 3 Comparison between the suggested filtenna and published studies

Refs.	Range of operating frequencies (GHz)	Tuning band (GHz)	Size (mm²)	Tuning mechanism
[35]	9.5–13	3.5	30 × 30	Mechanically switches
[36]	2.37–3.69	1.33	45 × 42.5	Single varactor diode
[37]	2.2–3.4	1.2	80 × 100	Single varactor diode
[38]	1.1–2.35	1.25	80 × 129	Ten pin diodes
[39]	6.16–6.6	0.44	30 × 59.8	Single varactor diode
[40]	3.9–4.82	0.92	20 × 62	Two varactor diodes
Proposed filtenna	6.45 to more than 12	5.55	45 × 35	Mechanically switches

for Case-01000001. Commonly, an acceptable agreement between the measured and simulated results was detected for all switching states. However, the slight discrepancy among predicted and measured results is due to fabrication and measurement setup tolerances. Table 3 compares the performance of the proposed filtenna to a recently published study. It is evident that the suggested filtenna has a more compact construction and a wider tunable band when compared to existing filtennas. Mechanically switches is used, which is another advantage.

4 Design of the MIMO filtenna

In a communication system implementing diversity, the same data are sent over independent fading paths. The signals received over the independent paths are then combined in such a way that the fading of the resultant signal is reduced. A wireless communication system equipped with diversity antennas leads to improved capacity and quality of the wireless channel.

In this section, a pattern diversity antenna with a frequency tuning feature (MIMO filtenna) is presented. Figure 14a shows the MIMO filtenna's structural layout. Two filtenna elements are used in the MIMO system, and they are positioned orthogonally with respect to one another. To perform well, this organization lowers the level of isolation. In the design, port 1 and port 2 are the MIMO ports. Consequently, MCs between port i and port j (S_{ij}), $i, j = 1, 2, i \neq j$ are minimized. Figure 14b shows the scattering parameter of the proposed MIMO filtenna without DS. S11 is -45 db at resonance frequency 7.55 GHz and S12 is -30 dB.

5 Results and discussion

Figure 15 depicts the MIMO structure's surface current distribution when one port is activated and the other is closed. One may observe that when one port is activated, the other ports also experience a certain amount of current. As a result, coupling requires greater reduction, which will enhance isolation. To achieve this, a special decoupling structure (DS) to support isolation between the antenna parts is recommended.

The core of the DS idea is the creation of a metamaterial structure (like zigzag) that is sandwiched between the MIMO antenna parts, supposedly suppressing all energy. To reduce the implantation area and achieve good isolation between the MIMO parts, the high impedance wire is meandering in a zigzag pattern. Figure 16a presents the geometry of the final structure of the proposed two-port MIMO filtenna together
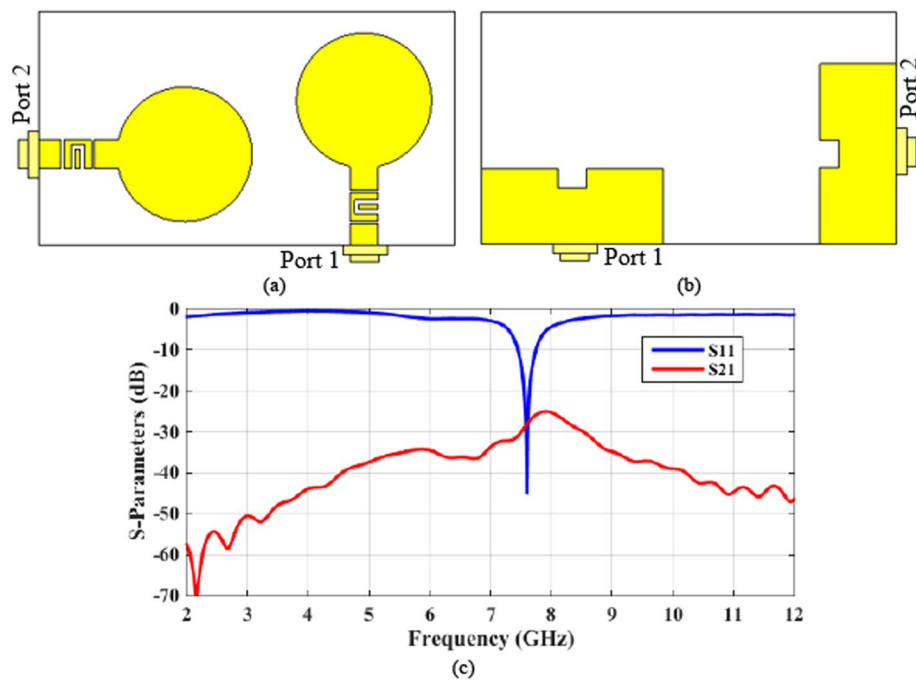
Fig.14 Geometry of the proposed MIMO filtenna without DS. **a** topview. **b** bottomview. **c** S-Parameters of the proposed MIMO filtenna without DS
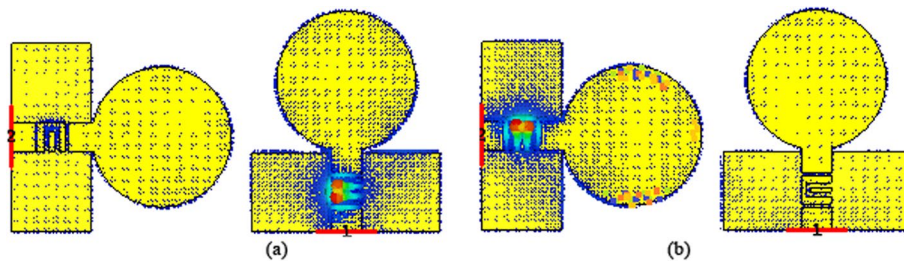

Fig.15 The suggested MIMO elements' surface current distribution when **a** excited port 1 and **b** excited port 2

with specific parameters. The two-port MIMO filter described is 80×45 mm^2 in size overall. Figure 16b shows the scattering parameter of the proposed MIMO filtenna without DS. S11 is -45 db at resonance frequency 7.55 GHz and S12 is -65 dB.

A comparison of isolation levels for instances with and without the DS is shown in Fig. 17. The proposed DS significantly minimizes the MC between antenna ports, which is noteworthy. Only port 1's findings are shown due of the symmetry. At 7.55 GHz, the coupling between port 1 and port 2 (S_{12}) is less than -20 dB for the case without DS. At 7.55 GHz, an improvement of around 40 dB is made with the DS, as depicted in Fig. 17. The distribution of surface current is examined for more proof. As seen in Fig. 18, Port (1) is individually energized at 7.55 GHz to study the DS effect. It has been shown that adding the proposed DS in between the antenna elements greatly reduces the current drift between them.
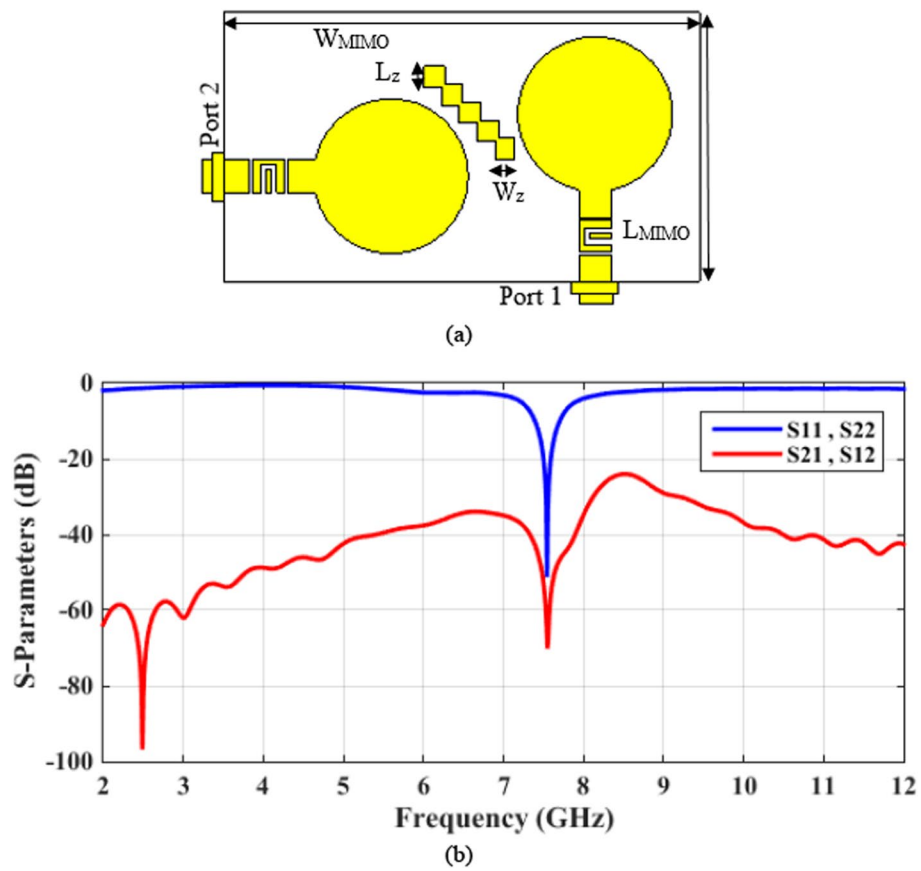
Fig.16 a The proposed MIMO filtenna's geometry with the DS. $W_{MIMO} = 80mm$, $L_{MIMO} = 45mm$, $W_z = L_z = 2.5mm$. **b** The suggested MIMO filtenna's S-parameters with DS
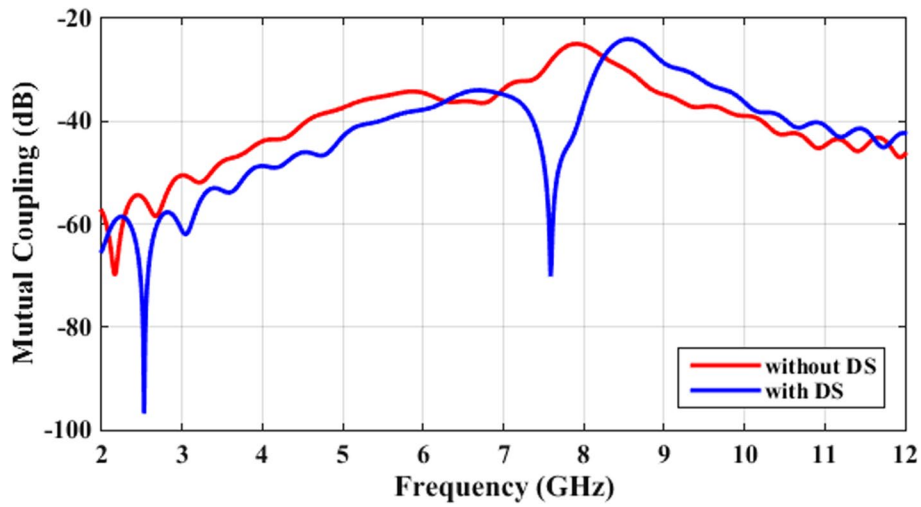

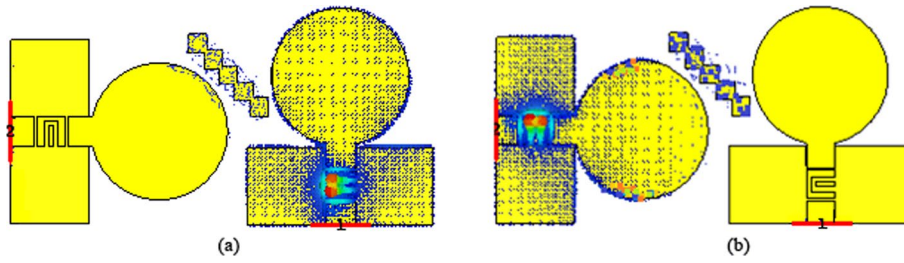**Fig. 17** Comparison of mutual coupling with and without DS

Fig. 18 Surface current distribution at 7.55 GHz for the proposed MIMO filtenna when **a** Port (1) is excited, **b** Port (2) is excited

5.1 MIMO performance study

5.1.1 ECC

In a MIMO system, the relationship between antenna elements is reflected by the ECC [36, 41]. For the estimation of the ECC, the S_{ij} and S_{ji} are used. For optimal MIMO system performance, the ECC should be less than 0.5 [37, 39]. The following is an estimation of the ECC [40]:

$$\text{ECC} = \frac{\left| S_{11}^* S_{12} + S_{21}^* S_{22} \right|^2}{\left(1 - |S_{11}|^2 + |S_{21}|^2\right)\left(1 - |S_{22}|^2 + |S_{12}|^2\right)}$$

The far-field radiation pattern can also be used to determine the ECC in the manner shown below. [40]:

$$ECC = \frac{\left| \int\int \left[\overrightarrow{F}_1(\theta,\phi) * \overrightarrow{F}_2(\theta,\phi) \right] d\Omega \right|^2}{\int\int \left| \left[\overrightarrow{F}_1(\theta,\phi) \right] \right|^2 d\Omega \int\int \left| \left[\overrightarrow{F}_2(\theta,\phi) \right] \right|^2 d\Omega}$$

where $\overrightarrow{F}_1(\theta,\phi)$ and $\overrightarrow{F}_2(\theta,\phi)$ are the field patterns of two filtenna elements, when port (1) and port (2) are activated, respectively. θ, ϕ and Ω are solid angles, and the Hermitian product is indicated by the asterisk (*). The simulated ECC of the suggested MIMO system for the two instances with and without the DS is shown in Fig. 19a. Without the DS, the MIMO antenna's maximum ECC is equal to 0.00012, whereas with the DS, it is equivalent to 2.4e−6.

5.1.2 Diversity gain (DG)

The DG is alternative pointer for the diversity level. A high value is necessary for effective isolation. (5) [42] can be used to estimate it.

$$\text{DG} = \sqrt{1 - \text{ECC}^2}$$

The DG for the proposed MIMO filtenna is greater than 9.9 in both circumstances, as shown in Fig. 19b.
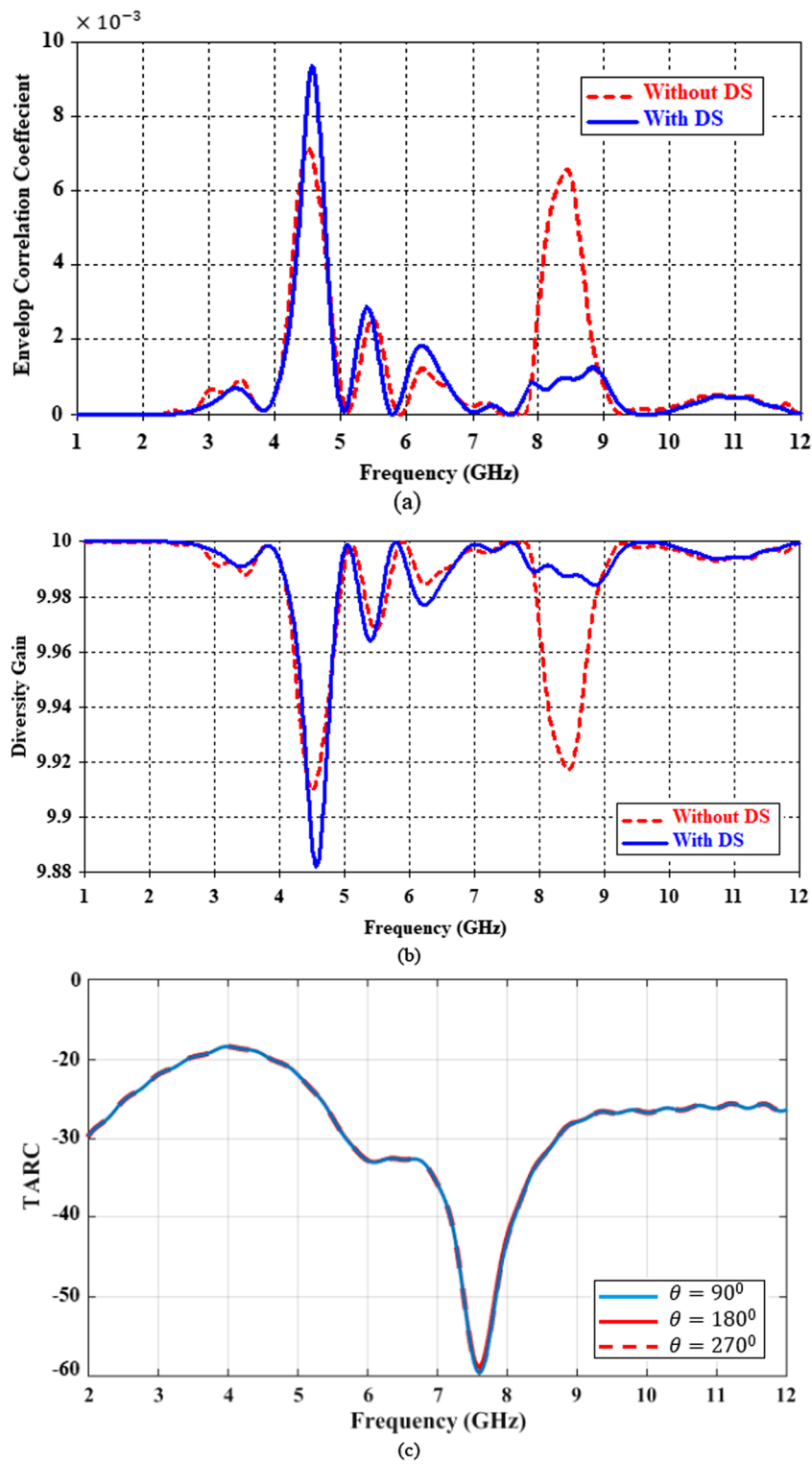
Fig. 19 The simulated MIMO parameters **a** ECC, **b** DG, and **c** TARC

5.1.3 Total active reflection coefficient (TARC)

The square root of the entire reflected power divided by the square root of the entire incident power is known as the TARC. Equation (6) is used to estimate it [24], and [43]. S-parameter curves converge as illustrated in Fig. 19c by inferring to the first port signal phase and altering the remaining port signal phases by three distinct values: 90°, 180°, and 270°. Over the whole working bandwidth, various signal phase variations perform effectively.

$$\Gamma_a^t = \frac{\sqrt{\left|(S_{11} + S_{12}e^{j\theta})\right|^2 + \left|(S_{21} + S_{22}e^{j\theta})\right|^2}}{2}$$

5.2 Manufacture and measurement

Fabricated and measured MIMO filtenna proposed. The fabricated MIMO filtenna is depicted in Fig. 20a. The measuring setup for the measurements of the S-parameters and the radiation pattern is shown in Fig. 20b, c. A comparison of the simulated and measured VSWR and scattering characteristics is shown in Fig. 21. The simulation and measurements show excellent agreement. Figure 22 depicts the radiation patterns for the x–y and y–z planes at 7.55GHz, respectively. In the y–z plane, the radiation pattern is infinity shaped, whereas in the x–y plane, it is omnidirectional. Figure 23 presents an illustration of gain over frequency. A gain of 6 dBi maximum is attained.
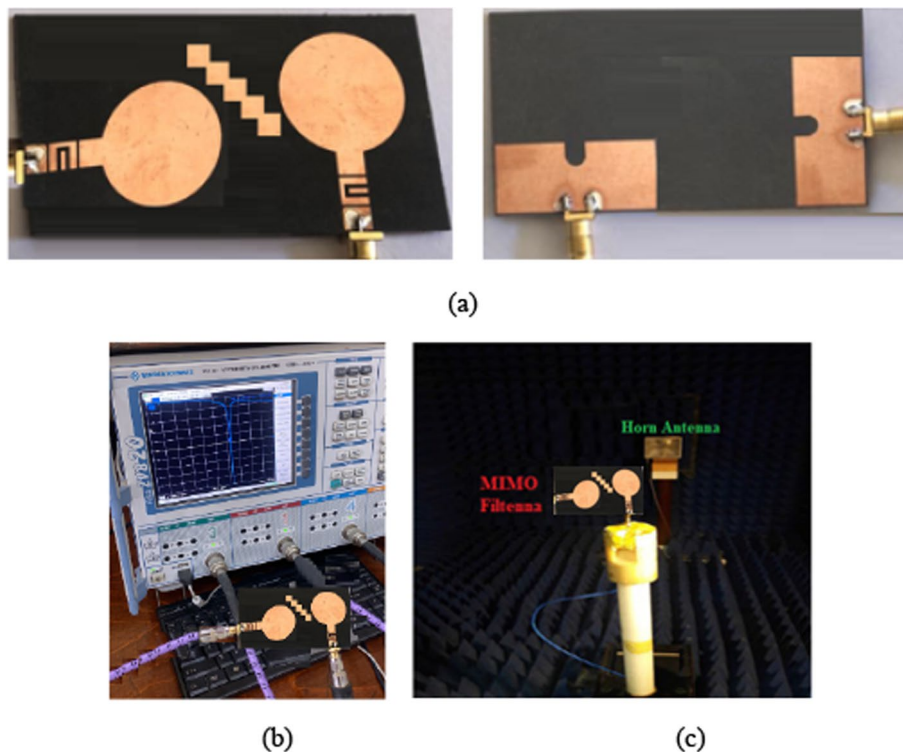

Fig. 20 a A MIMO antenna that was made. **b** The setup for measuring S-Parameters. **c** The setup for measuring radiation patterns
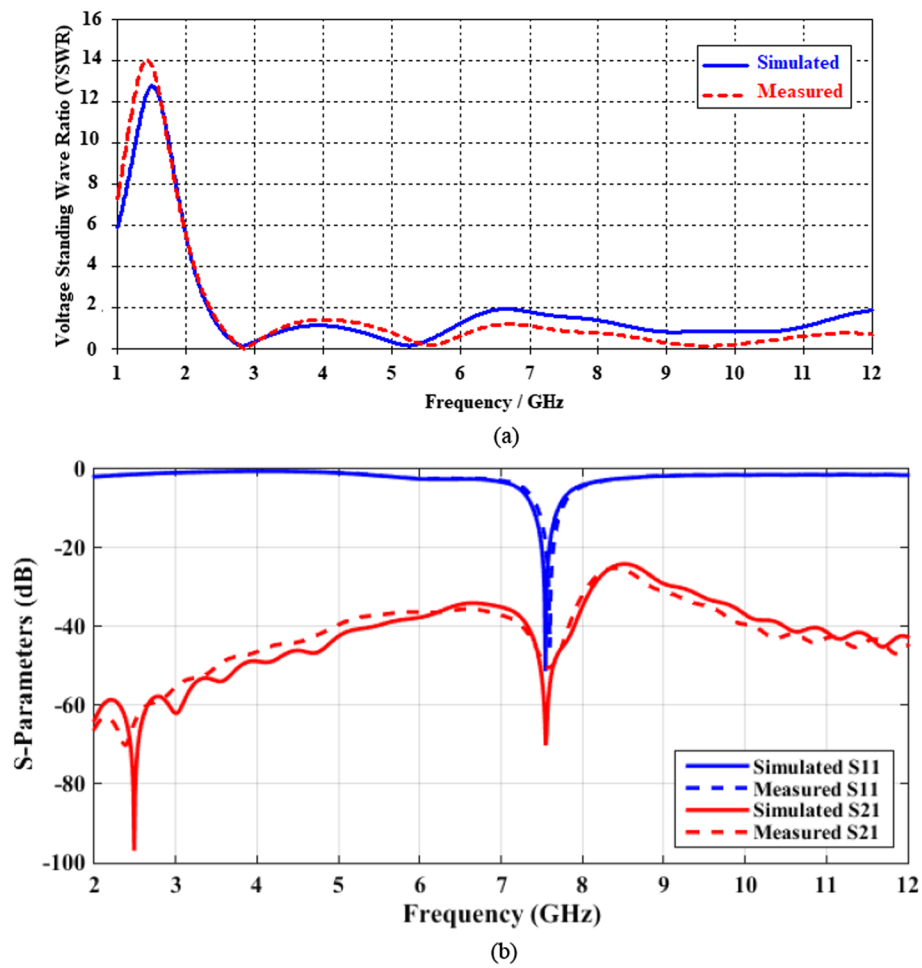
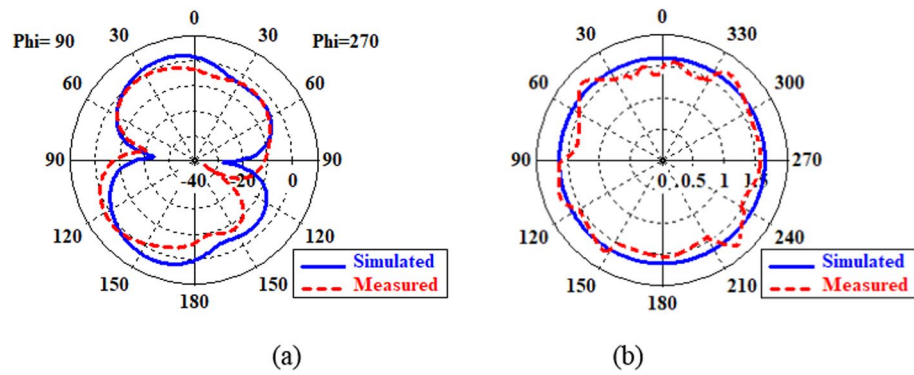**Fig. 21** An evaluation of the simulated and measured **a** VSWR, **b** Scattering parameters

Fig. 22 The proposed MIMO filtenna's simulated and measured y–z and x–y radiation patterns **a** y–z at 7.55 GHz, **b** x–y at 7.55 GHz
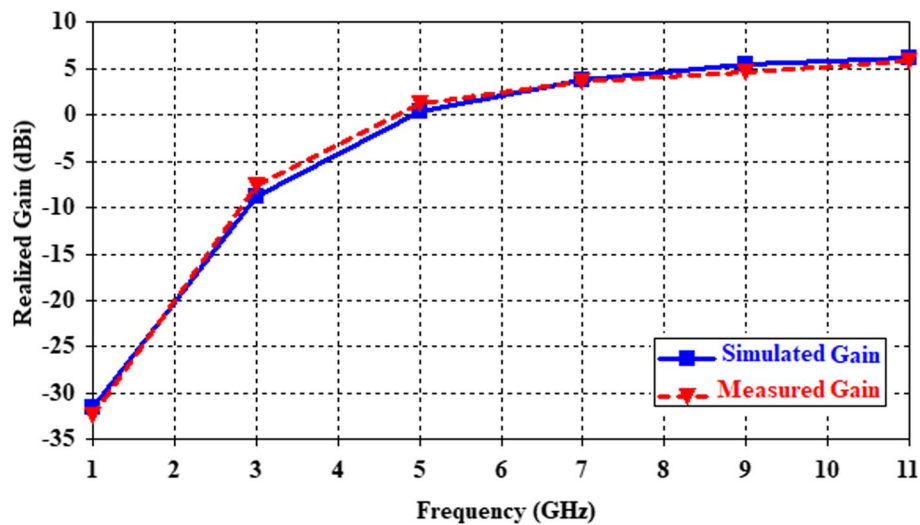
Fig. 23 Simulated and measured gain of proposed MIMO filtenna

Table 4 Comparison among the suggested MIMO filtenna and the literary work

Refs.	Size (mm^2)	No. of port	Bandwidth (GHz)	ECC	DG	MC	Gain (dBi)
[26]	65 × 50	2	1.2–6	0.1	9.96	− 25	< 4
[31]	55 × 60	2	3.45–3.55	–	–	− 20	5.8
[42]	75.19 × 75.19	4	3.1–17.3	0.1	–	− 14.5	5.5
[24]	32 × 64	2	3.1–10.6	< 0.02	–	− 17	4
Proposed work	80 × 45	2	7.4–7.75GHz	2.4e-6	9.9999	− 76	6

Table 4 provides a comparison of previously published literary works. The best element-to-element isolation, highest peak gain, and comparatively small size are displayed by the proposed MIMO filtenna. Also, among all literary works, the ECC and DG are the best.

6 Conclusion

A brand-new, small, circular antenna with an impedance bandwidth of 2.4 to more than 12 GHz has been created. For C-band applications, a filtenna with tunable frequencies from 6.45 to 8 GHz and from 8 to 12 GHz for X-band applications was built. A dual-port MIMO antenna with a surface area of 80×45 mm^2 has been used. The isolation between ports has been improved using orthogonal polarization and a metamaterial. It has proven possible to achieve a MIMO filtenna with an impedance bandwidth of 7.4–7.75 GHz, an isolation level of 76 dB, a peak gain of 6 dBi, and an ECC lower than 2.4e−6. The MIMO filtenna has been made up and measured. The modeling and measurements have achieved good agreement.

Declarations

Ethical approval and consent to participate

Not applicable.

Consent for publication

Author agree to publish the research in this journal.

Competing interests

The author declares no competing interests.

References

1. B. Razavi, Challenges in the design of cognitive radios, in *Proceedings of the IEEE Custom Integrated Circuits Conference* (CICC '09), San Jose, 2009, pp. 391–398
2. W.A. Awan, N. Hussain, S. Kim, N. Kim, A frequency-reconfigurable filtenna for GSM, 4G-LTE, ISM, and 5G sub-6 GHz band application. Sensors **22**(15), 5558 (2022). https://doi.org/10.3390/s22155558
3. A. S. A. El-Hameed, D. A. Salem, E. A. Abdallah, H. H. Abdullah, and E. A. Hashish, Design of dual frequency notched semicircular slot antenna with semicircular tuning stub, in *Proc. PIERS*, 2012, pp. 598–602
4. P. P. Shome and T. Khan, A novel filtenna design for ultra-wideband applications, in *Proc. IEEE MTT-S Int. Microw. RF Conf. (IMaRC)*, 2018, pp. 1–4. doi: https://doi.org/10.1109/IMaRC.2018.8877101
5. B.E. Carey-Smith, P.A. Warr, P.R. Rogers, M.A. Beach, G.S. Hilton, Flexible frequency discrimination subsystems for reconfigurable radio front ends. EURASIP J. Wirel. Commun. Netw. **2005**(3), 354–363 (2005)
6. W.T. Li, Y.Q. Hei, P.M. Grubb, X.W. Shi, R.T.I. Chen, Printing of wideband stacked microstrip patch array antenna on ultrathin flexible substrates. IEEE Trans. Compon. Packag. Manuf. Technol. **8**, 1695–1701 (2018)
7. H. Liu, P. Wen, S. Zhu, B. Ren, X. Guan, H. Yu, Quad-band CPW-fed monopole antenna based on flexible pentangle-loop radiator. IEEE Antennas Wirel. Propag. Lett. **14**, 1373–1376 (2015)
8. A. Al-Adhami, E. Ercelebi, A flexible metamaterial based printed antenna for wearable biomedical applications. Sensors **21**, 7960 (2021)
9. R.H. Elabd, H.H. Abdullah, M. Abdelazim, A. Abo talb, A. Shaban, Studying the performance of linear precoding algorithms based on millimeterwave MIMO communication system. Int. J. Sci. Eng. Res. (IJSER) **10**(1), 2076–2082 (2019)
10. R.H. Elabd, H.H. Abdullah, M. Abdelazim, A. Abo, talb, A. Shaban, Low complexity high- performance precoding algorithms for mm-wave MU-MIMO communication system. Wirel. Pers. Commun. (2020). https://doi.org/10.1007/s11277-020-07692-6
11. R.H. Elabd, A.J.A. Al-Gburi, SAR assessment of miniaturized wideband MIMO antenna structure for millimeter wave 5G smartphones. Microelectron. Eng. **282**, 112098–112115 (2023). https://doi.org/10.1016/j.mee.2023.112098
12. M.V. Berry, Z.V. Lewis, J.F. Nye, On the Weierstrass-Mandelbrot fractal function. Proc. R. Soc. Lond. Ser. A **370**(1743), 459–484 (1980)
13. E. Guariglia, Entropy and fractal antennas. Entropy **18**(3), 84 (2016)

14. R.C. Guido, S. Barbon, L.S. Vieira, F.L. Sanchez, C.D. Maciel, Introduction to the discrete shapelet transform and a new paradigm: joint time-frequency-shape analysis, in *IEEE International Symposium on Circuits and Systems* (IEEE ISCAS 2008), Seattle, 2008, vol. 1, pp. 2893–2896

15. E. Guariglia, S. Silvestrov, Fractional-wavelet analysis of positive definite distributions and wavelets on D'(C). in *Engineering Mathematics II*, (Springer, 2016), pp. 337–353

16. K.C. Hwang, A modified sierpinski fractal antenna for multiband application. IEEE Antennas Wirel. Propag. Lett. **6**, 357–360 (2007)

17. E. Guariglia, Harmonic sierpinski gasket and applications. Entropy **20**(9), 714 (2018)

18. E. Guariglia, R.C. Guido, Chebyshev wavelet analysis. J. Funct. Spaces **1**, 5542054 (2022)

19. A. Sibille, C. Oestges, A. Zanella, *MIMO from theory to implementation*, 1st edn. (Elsevier, San Diego, 2010)

20. X. Chen, S. Zhang, Q. Li, A review of mutual coupling in MIMO systems. IEEE Access **6**, 24706–24719 (2018)

21. A. Dkiouak, A. Zakriti, M. El Ouahabi, Design of a compact dual-band MIMO antenna with high isolation for WLAN and X-band satellite by using orthogonal polarization. J. Electromagn. Waves Appl. **34**(9), 1254–1267 (2020)

22. R.H. Elabd, H.H. Abdullah, M. Abdelazim, Compact highly directive MIMO vivaldi antenna for 5G millimeter-wave base station. J. Infrared Millim. Terahertz Waves (2021). https://doi.org/10.1007/s10762-020-00765-4

23. P. Prabhu, S. Malarvizhi, Novel double-side EBG based mutual coupling reduction for compact quad port UWB MIMO antenna. AEU- Int. J. Electron. Commun. **109**, 146–156 (2019)

24. N. Kumar, K.U. Kiran, Meander-line electromagnetic bandgap structure for UWB MIMO antenna mutual coupling reduction in E-plane. AEU-Int. J. Electron. Commun. **127**, 153423 (2020)

25. R.H. Elabd, H.H. Abdullah, A high isolation UWB MIMO vivaldi antenna based on CSRR-NL for contemporary 5G millimeter-wave applications. J. Infrared Milli Terahz Waves (2022). https://doi.org/10.1007/s10762-022-00894-y

26. S. Pahadsingh, S. Sahu, An integrated MIMO filltenna with wide band-narrow band functionality. AEU-Int. J. Electron. Commun. **110**, 152862 (2019)

27. I.S. Masoodi, I. Ishteyaq, K. Muzaffar, M.I. Magray, A compact band-notched antenna with high isolation for UWB MIMO applications. Int. J. Microw. Wirel. Technol. **13**(6), 634–640 (2021)

28. A. Dkiouak, A. Zakriti, M. El Ouahabi, A. Mchbal, Design of two element wi-MAX/WLAN MIMO antenna with improved isolation using a short stub-loaded resonator (SSLR). J. Electromagn. Waves Appl. **34**(9), 1268–1282 (2020)

29. M.M. Hassan, M. Rasool, M.U. Asghar, Z. Zahid, A.A. Khan, I. Rashid, A. Rauf, F.A. Bhatti, A novel UWB MIMO antenna array with band notch characteristics using parasitic decoupler. J. Electromagn. Waves Appl. **34**(9), 1225–1238 (2020)

30. Z. Li, Z. Du, M. Takahashi, K. Saito, K. Ito, Reducing mutual coupling of MIMO antennas with parasitic elements for mobile terminals. IEEE Trans. Antennas Propag. **60**(2), 473–481 (2012)

31. M. Abdullah, Q. Li, W. Xue, G. Peng, Y. He, X. Chen, Isolation enhancement of MIMO antennas using shorting pins. J. Electromagn. Waves Appl. **33**(10), 1249–1263 (2019)

32. S. Luo, Y. Li, Y. Xia, L. Zhang, A low mutual coupling antenna array with gain enhancement using metamaterial loading and neutralization line structure. Appl. Comput. Electromagn. Soc. J. **34**(3), 1–8 (2019)

33. X.-T. Yuan, W. He, K.-D. Hong, C.-Z. Han, Z. Chen, T. Yuan, Ultra- wideband MIMO antenna system with high element-isolation for 5G smartphone application. IEEE Access **8**, 56281–56289 (2020)

34. G.-S. Lin, C.-H. Sung, J.-L. Chen, L.-S. Chen, M.-P. Houng, Isolation improvement in UWB MIMO antenna system using carbon black _lm. IEEE Antennas Wirel. Propag. Lett. **16**, 222–225 (2017)

35. R.A. Youssef, M.A. Mohamed, A. Kabeel, Evaluation of energy detection-based spectrum sensing for cognitive radio applications. Mansoura Eng. J. (MEJ) **47**(6), 1–10 (2022)

36. H.S. Fouda, A.H. Abdullah, Practical implementation of real-time cognitive radio energy detector using frequency reconfigurable filltenna. J. Electromagn. Appl. **34**(2), 168–182 (2019). https://doi.org/10.1080/09205071.2019.1692699

37. J. Araujo, M. Oliveira, F.P. Cavalcanti, C. Silva, M.S. Coutinho et al., Reconfigurable filltenna using varactor diode for wireless applications. J. Microw. Optoelectron. Electromagn. Appl. **20**(4), 834–854 (2021)

38. L. Ge, K.M. Luk, A band-reconfigurable antenna based on directed dipole. IEEE Trans. Antenna Propag. **64**, 64–71 (2014)

39. Y. Tawk, J. Costantine, C. Christodoulou, A varactor-based reconfigurable filltenna. IEEE Antenna Wirel. Propag. Lett. **11**, 716–719 (2012)

40. Y. Qin, F. Wei, Y. Guo, A wideband-to-narrowband tunable antenna using a reconfigurable filter. IEEE Trans. Antenna Propag. **63**, 2282–2285 (2015)

41. L.G. Silva, A.A.C. Alves, A. CerqueiraSodré, Optically Controlled Reconfigurable Filltenna. Int. J. Antennas Propag. (2016). https://doi.org/10.1155/2016/7161070

42. A. Kayabasi, A. Toktas, E. Yigit, K. Sabanci, Triangular quad-port multi-polarized UWB MIMO antenna with enhanced isolation using neutralization ring. AEU-Int. J. Electron. Commun. **85**, 47–53 (2018)

43. S. Pahadsingh, S. Sahu, An integrated MIMO filltenna with wide band- narrow band functionality. AEU-Int. J. Electron. Commun. **110**, 152862 (2019)

Publisher's Note

Springer Nature remains neutral with regard to jurisdictional claims in published maps and institutional affiliations.